



# Corrosion behaviour of zinc coated with composite silica layers incorporating poly(amidoamine)-modified graphene oxide

Tamara-Rita Ovari<sup>1</sup> · Gabriel Katona<sup>2</sup> · Maria Coros<sup>3</sup> · Gabriella Szabó<sup>2</sup> · Liana Maria Muresan<sup>1</sup>

Received: 1 October 2022 / Revised: 5 December 2022 / Accepted: 16 December 2022 / Published online: 23 December 2022  
© The Author(s), under exclusive licence to Springer-Verlag GmbH Germany, part of Springer Nature 2022

## Abstract

The aim of the paper is to carry out a detailed investigation of the effect of graphene oxide-poly(amidoamine) (GO-PAMAM) incorporated in silica matrices on the corrosion behaviour of zinc. GO was modified with PAMAM dendrimer in order to improve its dispersion in the silica coatings prepared on zinc by dip-coating. Morpho-structural and physico-chemical characterization of the graphenes were made by FT-IR and Raman spectroscopy, TEM, and XRD. After incorporation, the effect of graphenes on the anti-corrosive performance of silica-coated zinc was investigated by electrochemical impedance spectroscopy. The results revealed that GO-PAMAM nanosheets dispersed in silica matrix significantly improved the corrosion resistance of the coatings. The polarization resistance  $R_p$  increased from 680 to 2489 k $\Omega$  cm<sup>2</sup>. The performances of SiO<sub>2</sub>-GO-PAMAM coatings were compared with those of SiO<sub>2</sub> coatings incorporating GO, reduced graphene oxide (rGO), and 3-aminopropyl triethoxysilane (APTES)-modified GO. The influence of silica sol-ageing of the composite coatings was also investigated, as the polycondensation plays an important role in its anti-corrosive properties. The morphology of the composite coatings was examined by SEM, and their wettability by contact angle measurements. The protection offered by the SiO<sub>2</sub>-GO-PAMAM composite material is the leading. This can be associated with the GO-PAMAM's high oxidation degree, low electrical conductivity, and by the fact that reduces the penetration of the electrolyte into the silica/zinc interface.

**Keywords** Sol-gel · Silica coating · PAMAM-modified graphene oxide · Corrosion · Electrochemical impedance spectroscopy · Sol-ageing

## Introduction

Silica (SiO<sub>2</sub>) coatings are widely used on metals to mitigate corrosion because of their tolerance to high temperatures, sunlight, and physical degradation. Advantages such as transparency, good chemical resistance, high flexibility, and good impact resistance are among the known benefits of the

latter. The hydrolysable siloxane groups of silane molecules form strong covalent bonds with the substrate, generating excellent adhesion between the Zn surface and SiO<sub>2</sub> coating [1]. Despite the fact that silane films are quite hydrophobic, they fall short in offering long term protection, because of their tendency to form microforms, cracks, but also it is known that they possess low cross-linked areas [2, 3]. As progress has been made in the field of sol-gel based coatings, incorporation of nanofillers into the coating's structure appeared in order to improve the coating's protective properties [4]. An increased performance of their barrier properties can be achieved by the hydrofobization of their surface [5]. Furthermore, introducing various surfactant templates in the precursor sol [5, 6] mesoporous texture can be developed, making them suitable for corrosion inhibitor carriers and eventually to gain self-healing properties.

Among the filler materials, graphene oxide (GO) should represent an adequate candidate. GO is a nanomaterial thought to improve the mechanical properties of polymeric coatings by lengthening the electrolyte pathway and

✉ Liana Maria Muresan  
liana.muresan@ubbcluj.ro

<sup>1</sup> Department of Chemical Engineering, Faculty of Chemistry and Chemical Engineering, Babes-Bolyai University, 11, Arany J. St., Cluj-Napoca-Napoca 400028, Romania

<sup>2</sup> Department of Chemistry and Chemical Engineering, Hungarian Line, Faculty of Chemistry and Chemical Engineering, Babes-Bolyai University, 11 Arany J. St., Cluj-Napoca-Napoca 400028, Romania

<sup>3</sup> National Institute for Research and Development of Isotopic and Molecular Technologies, Donath Street No. 67-103, P.O. BOX 700, Cluj-Napoca-Napoca, Romania

decreasing the porosity of the coatings [7]. This is due to their well-defined structure, high surface area, and small particle size [8]. However, major difficulties may occur with the dispersion of the GO nanosheets in polymer matrices. The nanoparticle tendency to form agglomerates due to their large surface area and surface energy [9] provides obstacles in achieving great results. The simplest and most efficient way to prevent the agglomeration of the nanoplatelets is through chemical functionalization [10]. Various studies have investigated the chemical functionalization of GO [9, 11], which is achievable thanks to the hydroxyl, carboxyl and epoxy groups found on its basal plane and edges [7]. Some of the utilized modifications were carried out by titanate  $\text{TiO}_3^{2-}$  coupling agent [12], inorganic nano-oxides ( $\text{ZnO}$ ,  $\text{TiO}_2$ ) [13, 14], corrosion inhibitors (amino-azobenzene, diamino-azobenzene, metronidazole) [9, 15], silane coupling agents (APTES) [1, 7, 16, 17], and PAMAM dendrimer [10, 18].

The lamellar structure of GO can be penetrated by the spherical structure of the PAMAM dendrimer which results in a more exfoliated structure. Moreover, PAMAM also prevents the agglomeration of GO and improves dispersion stability. These amines form covalent bonding with the carboxylic and epoxide groups of GO [10].

On other note, it was reported that graphene could have a corrosion promoting activity when in contact with the metal, because of electron transfer. According to some published reports, this can be suppressed by the isolation layer effect of APTES [9]. Furthermore, by functionalization, the electrical conductivity of graphene has been observed to decrease considerably [11].

It is well known that the preparation of high thickness sol–gel based anticorrosive coatings remains a great challenge, due to the formation of cracks and defects formation when thicker inorganic sol–gel layers are deposited on the substrate [2].

As mentioned above, various nanofillers and nanoparticles have been used in order to improve the protective properties of silane sol–gel coatings, but there are few published data regarding the GO nanosheets effect on the performance of silane coatings [17]. So far as we know, GO-PAMAM nanoparticles were embedded only in epoxy coatings, and there is no published literature regarding the effect of GO-PAMAM incorporated in silica matrices, nor a comparative study of rGO, GO, GO-APTES, GO-PAMAM and of  $\text{SiO}_2$  sol-ageing impact, on the composite silica coatings' anti-corrosive properties.

In this context, the aim of the paper is to carry out a detailed investigation of the composite silica coatings incorporating GO-PAMAM, mainly by electrochemical methods and morpho-structural characterizations, and to compare the performances of the new silica-based coatings with those containing GO, reduced GO (rGO), and GO-APTES, respectively.

## Materials and methods

### Materials

For the preparation of the silica precursor sol, tetraethyl-orthosilicate (TEOS, for synthesis, > 99%, Merck), ethanol (EtOH, 99,3%, Chemical Company), distilled water, and hydrochloric acid (HCl, purum, 37%, Fluka) were used. The reduced graphene oxide (rGO) and the graphene oxide (GO) were purchased from the National Institute for Research and Development of Isotopic Molecular Technologies, Cluj-Napoca. For the modification of the GO, we used 3-aminopropyltriethoxysilane (APTES, 98%, Alfa Aesar), sodium hydroxide (NaOH, 97%, Lachema), and acetic acid glacial ( $\text{CH}_3\text{COOH}$ , 99,5% Chemical Company). For the modification with poly(amidoamine) 2<sup>nd</sup>-generation dendrimer (PAMAM G2.0, 38%, Dendritech), dimethylformamide (DMF, 99,5%, Thermo Scientific) and thionyl chloride ( $\text{SOCl}_2$ , 99%, Sigma-Aldrich) were used.

The Zn samples (purchased from Altdepozit, with 99% purity, containing reduced amounts of Ti and Cu), with dimensions of  $7 \times 2$  cm, polished with emery paper (grade 1500, 3000, 5000) were pretreated with 2-propanol (2-PrOH, 99,7%, Chemical Company) and 0.1 M aqueous HCl. The limitation of the surface to  $2 \text{ cm}^2$  was reached by using a transparent lacquer. This generated the active surface of the sample used in electrochemical measurements.

### Synthesis of GO

GO synthesis was realized by a modified Hummer's method, recently published [19].

For more efficient oxidation of natural graphite, a pre-oxidation step was introduced. The typical pre-oxidation procedure consists in adding the graphite (4.6 g) to a warm solution (80 °C) of concentrated sulfuric acid (8 mL), potassium persulfate (2.5 g), and phosphorus pentoxide (2.5 g). The mixture was next heated to 100 °C and left to slowly cool down. Then, 300 mL water was added to dilute the mixture. The suspension was filtered, washed until neutral pH, and dried at ambient temperature [19].

The oxidation step: to a suspension of pre-oxidized graphite powder (3.5 g) and sodium nitrate (1.6 g) in sulfuric acid (60 mL) cooled in an ice-water bath were slowly added 8 g of potassium permanganate. The temperature was not allowed to reach 10 °C. The next day, the mixture was warmed to 35 °C and kept for 1 h 45 min at this temperature. The suspension was diluted with 150 mL water, the temperature rising to 100 °C [19]. 100 mL of water were additionally added after 2 h. The reaction was stopped with hydrogen peroxide (30%) until the gas development was no longer observed. The mixture was filtered and washed with

a diluted HCl solution (250 mL, 1%). The obtained product was suspended in bidistilled water and dialysed for 5 days [20]. After that, we exfoliated the samples by 1 h sonication. The final material was obtained by lyophilization.

### Functionalization of GO by APTES

The functionalization of GO was accomplished through a hydrolysis-condensation sequence by the organosilane APTES. Prior to functionalization, the GO (0.031 g) was ultrasonicated for 1 h in 12.5 mL of aqueous solution. Another solution was prepared containing: 1.32 mL APTES, 0.3 mL water, and 29.65 mL ethanol. By mixing the two solutions, the next step was to adjust the pH value to 4.5 by addition of acetic acid under constant stirring for 2 h. After that, the pH was adjusted to 11 by the use of sodium hydroxide and the mixture was stirred for another hour at room temperature. The supernatant was removed by filtering the mixture, and the GO-APTES residue was washed with deionized water and ethanol (30:20 w/w) [1].

### Functionalization of GO by PAMAM Dendrimer

In order to modify the GO with PAMAM G2.0, it was necessary to activate the carboxyl groups found on the surface of GO, which leads to nucleophilic substitution. This step was realized with thionyl chloride  $\text{SOCl}_2$  and dimethylformamide (DMF) in a proportion of 0.15 g GO; 37.5 mL  $\text{SOCl}_2$ ; 0.6 mL DMF, by stirring at 70 °C for 24 h. After that, the mixture was filtered to remove excessive  $\text{SOCl}_2$ . The remained GO-COCl was then dispersed in 15 mL ethanol together with the PAMAM dendrimer. Eventually, the excessive amount of ethanol was removed by filtration and several water rinsing. The powder was then dried at 60 °C to generate GO-PAMAM [10].

### Precursor sol synthesis

The silica precursor sols based on acid catalyse (0.1 M aqueous HCl solution) were prepared from the controlled hydrolysis of TEOS in EtOH. The solution containing TEOS:EtOH:H<sub>2</sub>O:HCl (1:18.6:5.5:1  $10^{-3}$  M) was stirred for 1 h at ambient temperature, then kept for 24 h at 18–20 °C before usage.

### Preparation of silica/GO and silica/modified-GO nanocomposite coatings

Prior to layer deposition, the scratches found at the surface of the Zn substrate were removed by polishing with emery paper (800, 2000, 5000). The next step was the ultrasonication of the substrates in 2-propanol solution for 2 min, followed by treatment with 0.1 M aqueous HCl solution, and

finally with 2-propanol solution. Each time the wafer was blow-dried.

5 different silica sols were prepared: one containing rGO, the second GO, the third GO-APTES, and the fourth GO-PAMAM (each one had a concentration of 0.86 g/dm<sup>3</sup>). The last one did not contain any nanofillers and served as a reference. The silica sol was left for 1 day before usage or before adding the nanofillers with the scope that the silica network can be formed. The initial samples were immersed in the sols the moment the nanofillers were added and the sol was then ultrasonicated for 10 min. The other samples were coated from the silica sol and also from the silica sols containing rGO/GO/GO-APTES/GO-PAMAM after being kept at 18–20 °C for 1 week, 2, 3, 4, 6, and 8 weeks, respectively.

The silica nano-coatings were prepared from the above-mentioned precursor sols by using a homemade dip-coater and the sol-gel method. Immersed in the sols, the Zn wafers were withdrawn with a constant speed of 10 cm/min. The coated and uncoated Zn samples were cured at 150 °C for 1 h since it was proved that this is the optimal temperature and duration of the curing [21].

### Fourier transformed infrared spectroscopy

FT-IR spectra were recorded on a JASCO FT/IR-6800 spectrometer in the region 4000–500 cm<sup>-1</sup>. The preparation of the samples consisted of a simple step, just adding a small quantity of the solid samples.

### Transmission electron microscopy

TEM measurements were realized with a Hitachi H-7650 transmission electron microscope. The different graphene samples were diluted in methanol.

### Raman spectroscopy measurements

Raman spectroscopy was performed using an NTEGRA Spectra platform, placed on a NEWPORT RS4000 optical table with a vibration isolation system and equipped with a SOLAR TII confocal Raman spectrometer coupled with an Olympus IX71 microscope in two different configurations. Detection was achieved with a CCD camera (NT-MDT).

### X-ray crystallography

The X-ray powder diffraction (XRD) patterns were collected with a Bruker D8 Advance diffractometer, using  $\text{CuK}\alpha 1$  radiation ( $\lambda = 1.5406 \text{ \AA}$ ). To filter out the  $\text{K}\alpha 2$  radiation and to increase the resolution a Ge (111) monochromator in the incident beam was used.

## Electrochemical characterization

All measurements were carried out in a three-electrode cell, including a working electrode (the coated or bare Zn wafer,  $S = 2 \text{ cm}^2$ ), a reference electrode ( $\text{Ag}/\text{AgCl}/\text{KCl}_{\text{sat}}$ ) and a counter electrode (platinum wire), in  $0.2 \text{ g/L Na}_2\text{SO}_4$  solution ( $\text{pH} = 5.0$ ) with a computer-controlled potentiostat (PARSTAT 2737).

In the first step, the open circuit potentials (OCP) were recorded for 1 h. The electrochemical impedance spectroscopy (EIS) was performed within the frequency range of 10 kHz to 10 MHz and at 10 mV (peak to zero) amplitude of voltage, at OCP (number of points 30). Potentiodynamic polarization curves were recorded with a scan rate of 1 mV/min starting from a potential with  $-250 \text{ mV}$  lower than OCP.

The electrical circuit was fitted with the ZsimpWin programme. The reproducibility of the results was assured by the measurements of triplicate samples.

The inhibition efficiency of the systems was approximated using the following equation:

$$\text{IE}(\%) = 100 \cdot \frac{|Rp|_s - |Rp|_0}{|Rp|_s} \quad (1)$$

where  $|Rp|_0$  is the polarization resistance value of the bare Zn sample, and  $|Rp|_s$  is the polarization resistance of the coated samples.

## Coating thickness

The coating thickness was measured with an instrument BB25 purchased from Trotec, able to read layer thicknesses on surfaces by the eddy current method, with  $\pm 1\%$  accuracy. Each sample was measured 3 times, and an average value was calculated.

## Contact angle measurements

Contact angle measurements were performed in the coated zinc substrates to get information about the polarity of the coatings. The measurements were carried out in a closed sample chamber, in saturated atmosphere, with the same electrolyte used in the electrochemical measurements, namely  $0.2 \text{ g/L}$  aqueous  $\text{Na}_2\text{SO}_4$  solution with  $20 \mu\text{L}$  droplets.

The contact angle was calculated with the ImageJ programme, with  $\pm 0.1$  uncertainty.

## Scanning electron microscopy measurements

A Hitachi SU8230 ultra-high-resolution scanning electron microscope was used in order to study the morphological and structural properties of the  $\text{SiO}_2/\text{GO-PAMAM}$

coatings before and after immersion in  $\text{Na}_2\text{SO}_4$  electrolyte for 2 weeks, with or without sol-ageing, and also to compare the results to those of  $\text{SiO}_2$  coatings.

## Results and discussion

First, the modified GO nanosheets were characterized morpho-structurally and physico-chemically, by several methods.

### Fourier transformed infrared spectroscopy

In order to prove the modification of GO, FT-IR spectra of GO, rGO, GO-APTES, and GO-PAMAM nanoparticles were recorded as illustrated in Fig. 1 and examined.

The in-plane stretching vibration of  $\text{sp}^2$ -hybridized  $\text{C}=\text{C}$  found at  $1500\text{--}1600 \text{ cm}^{-1}$  can be observed in the case of the rGO spectra where the peaks are not overlapped. The GO increased signals representative for the oxidation groups are located at  $3162 \text{ cm}^{-1}$  corresponding to OH groups; at  $1710 \text{ cm}^{-1}$ , we can observe the stretching vibration of  $\text{C}=\text{O}$  specific to carboxyl groups; and at  $1220 \text{ cm}^{-1}$ , the presence of epoxide group ( $\text{C}-\text{O}-\text{C}$ ), whereas at  $1050 \text{ cm}^{-1}$  can be noticed the presence of alkoxy groups [22].

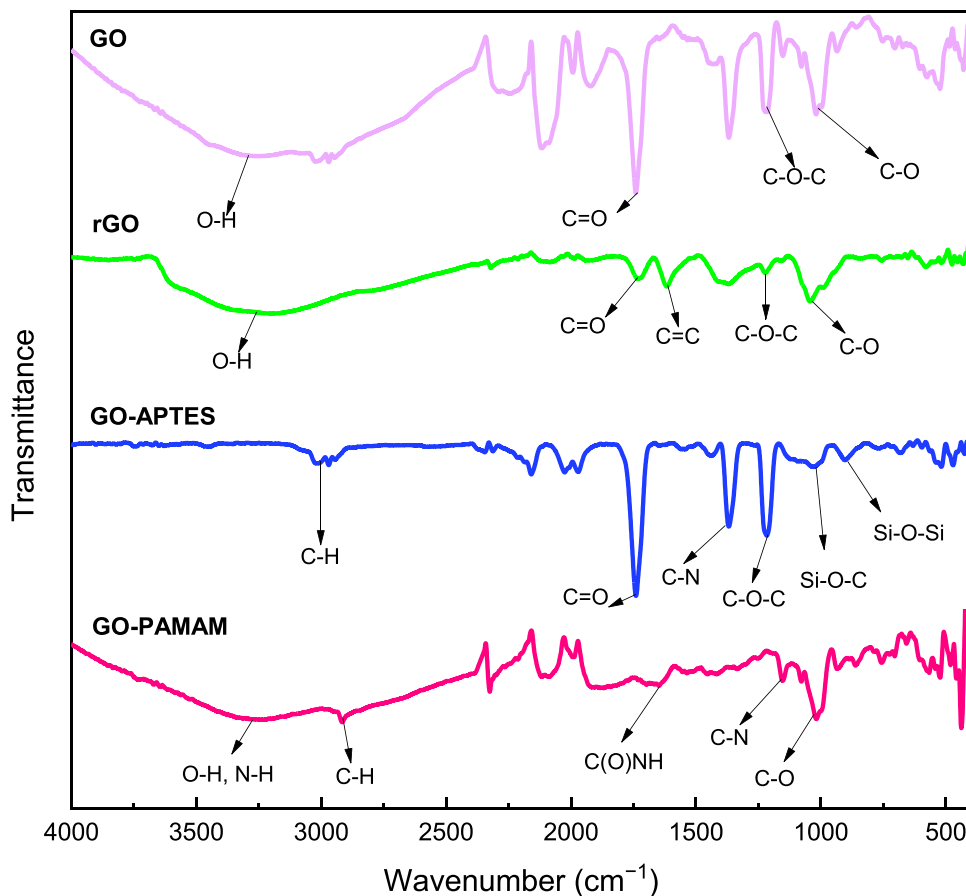
New bands become visible after interaction of GO with APTES; around  $1000 \text{ cm}^{-1}$ , the signal of  $\text{Si}-\text{O}-\text{C}$ , the  $\text{Si}-\text{O}-\text{Si}$  absorption peak shows the reaction between the APTES molecules. Nevertheless, the  $\text{C}-\text{OH}$  vibrations of hydroxy groups disappear in GO-APTES samples, which corroborates the fact the ethoxysilane groups of the APTES reacts with the OH of the GO releasing ethanol and forming  $\text{Si}-\text{O}-\text{C}$  bonds. It is also possible that the amine of the APTES reacts with the epoxy groups found on the surface of GO, but from the FT-IR spectra can be observed that the  $\text{C}-\text{O}-\text{C}$  signal remains visible in the case of GO-APTES. APTES molecules may react with each other creating a silica-like structure on the surface of the GO [23], with the appearance of a peak at around  $1000 \text{ cm}^{-1}$ .

In the case of PAMAM modified GO, a new band emerges at  $1650 \text{ cm}^{-1}$ , which can be attributed to the  $\text{N}-\text{H}$  bending vibrations of the amide groups. Furthermore, the characteristic absorption peak for carboxyl groups has vanished in the spectrum of GO-PAMAM [10], confirming that the reaction takes place between the amino groups of the dendrimer and the carboxyl groups of the GO. See the schematic representation of the GO synthesis in Fig. 2.

### Transmission electron microscopy

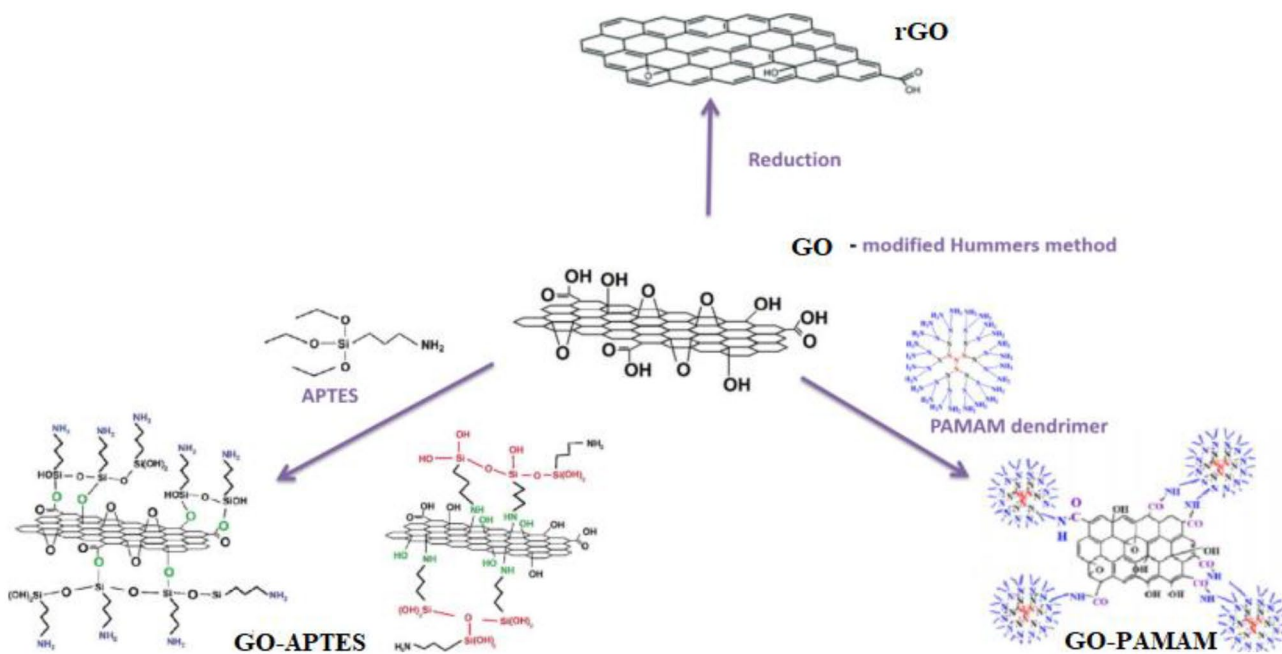
The TEM images (Fig. 3) reveal the characteristic morphology of the graphenes and confirm the successful functionalization

**Fig. 1** FT-IR spectra of GO, rGO, GO-APTES, and GO-PAMAM



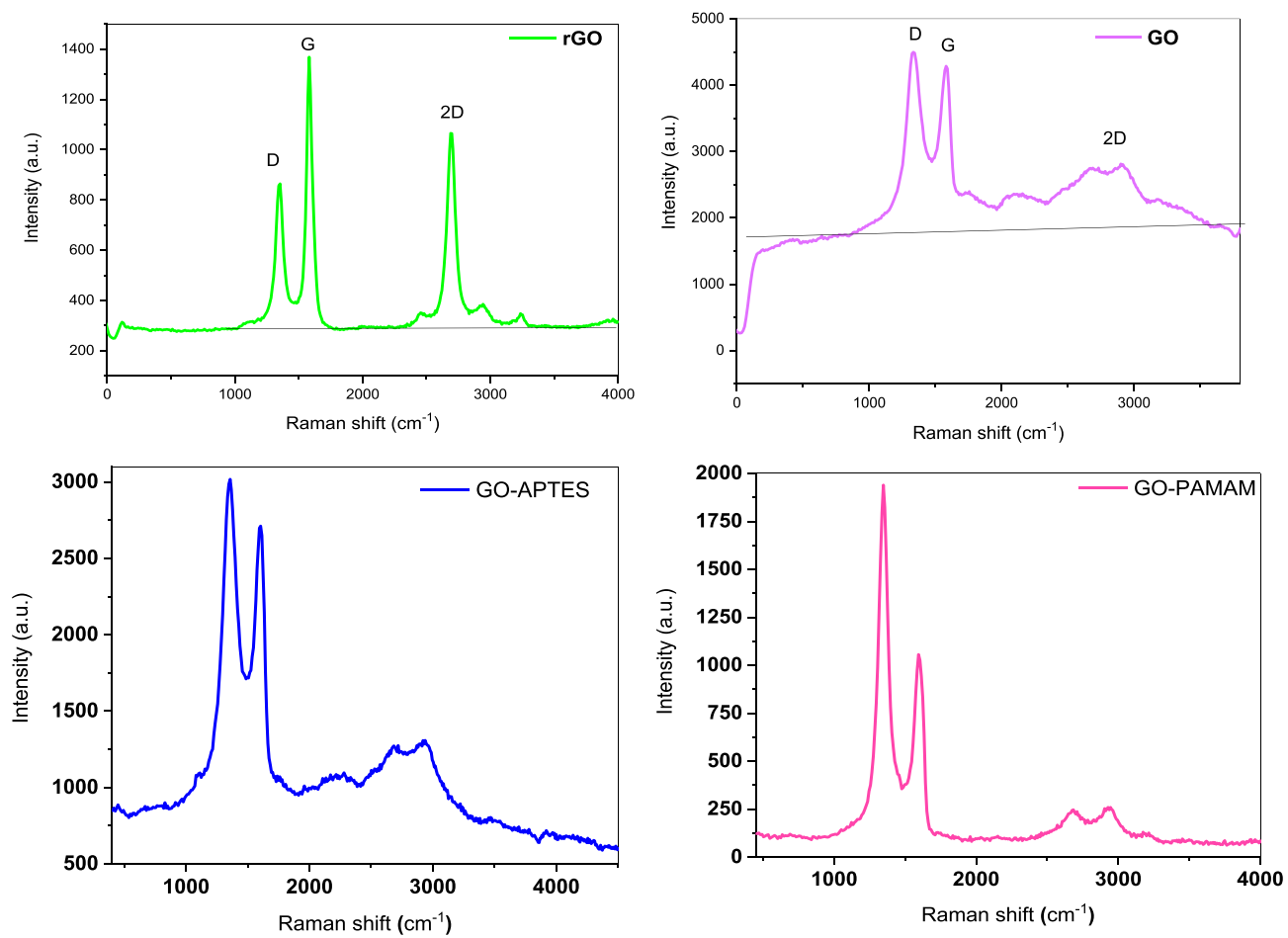
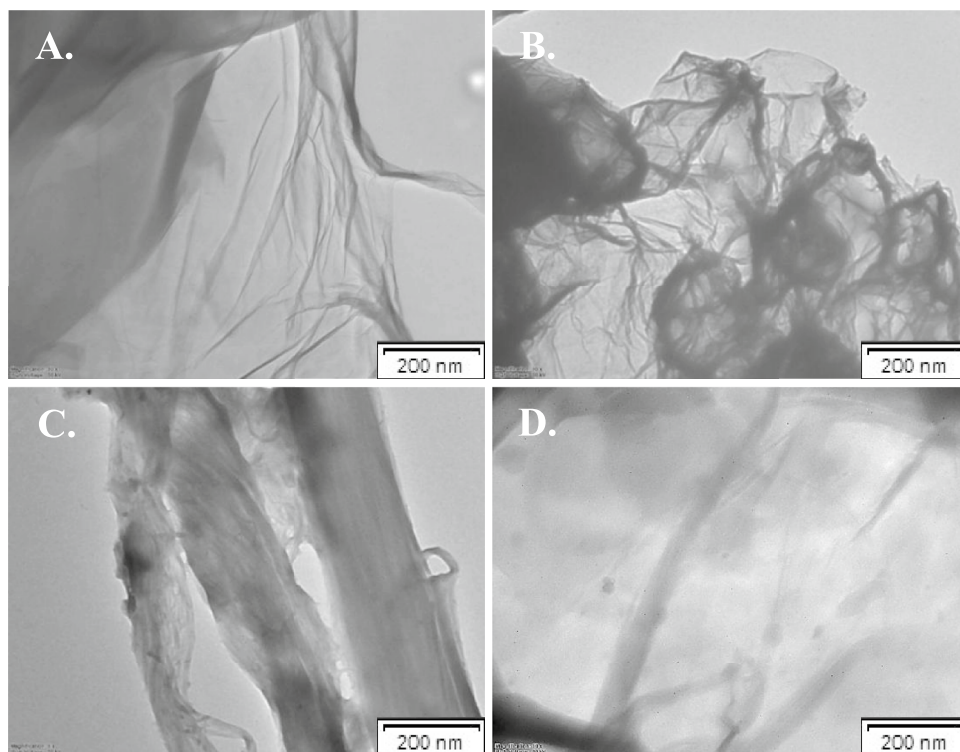
of GO with APTES and PAMAM. Besides, it can be observed that in the case of modified graphenes, especially the GO-APTES, the thin film of the graphene is torn apart by the

silane coupling agent forming threads. This means that the restacking of the particles was effectively interrupted.



**Fig. 2** Schematic representation of the GO synthesis

**Fig. 3** TEM images of GO (A), rGO (B), GO-APTES (C), and GO-PAMAM (D)



**Fig. 4** Raman spectra of rGO, GO, GO-APTES, and GO-PAMAM nanoparticles

**Table 1** The values of the Raman parameters obtained from the corresponding spectra of each sample

Sample	$G$ ( $\text{cm}^{-1}$ )	$D$ ( $\text{cm}^{-1}$ )	$I_G$ (a.u.)	$I_D$ (a.u.)	$I_D/I_G$	$L_a$ (nm)
rGO	1579	1348	1070	575	0.54	35.34
GO	1570	1333	2486	2741	1.1	17.23
GO-APTES	1604	1355	3007	2699	0.89	21.16
GO-PAMAM	1598	1349	1050	1933	1.84	10.32

The wrinkled surface of the GO provides stability and avoids collapse back to a graphitic structure. With a similar morphology, a thin extended film with wrinkles on it appears on the rGO [22]. The GO-PAMAM seems to have some black spots on the surface, that is attributed to the PAMAM molecules [24].

### Raman spectroscopy measurements

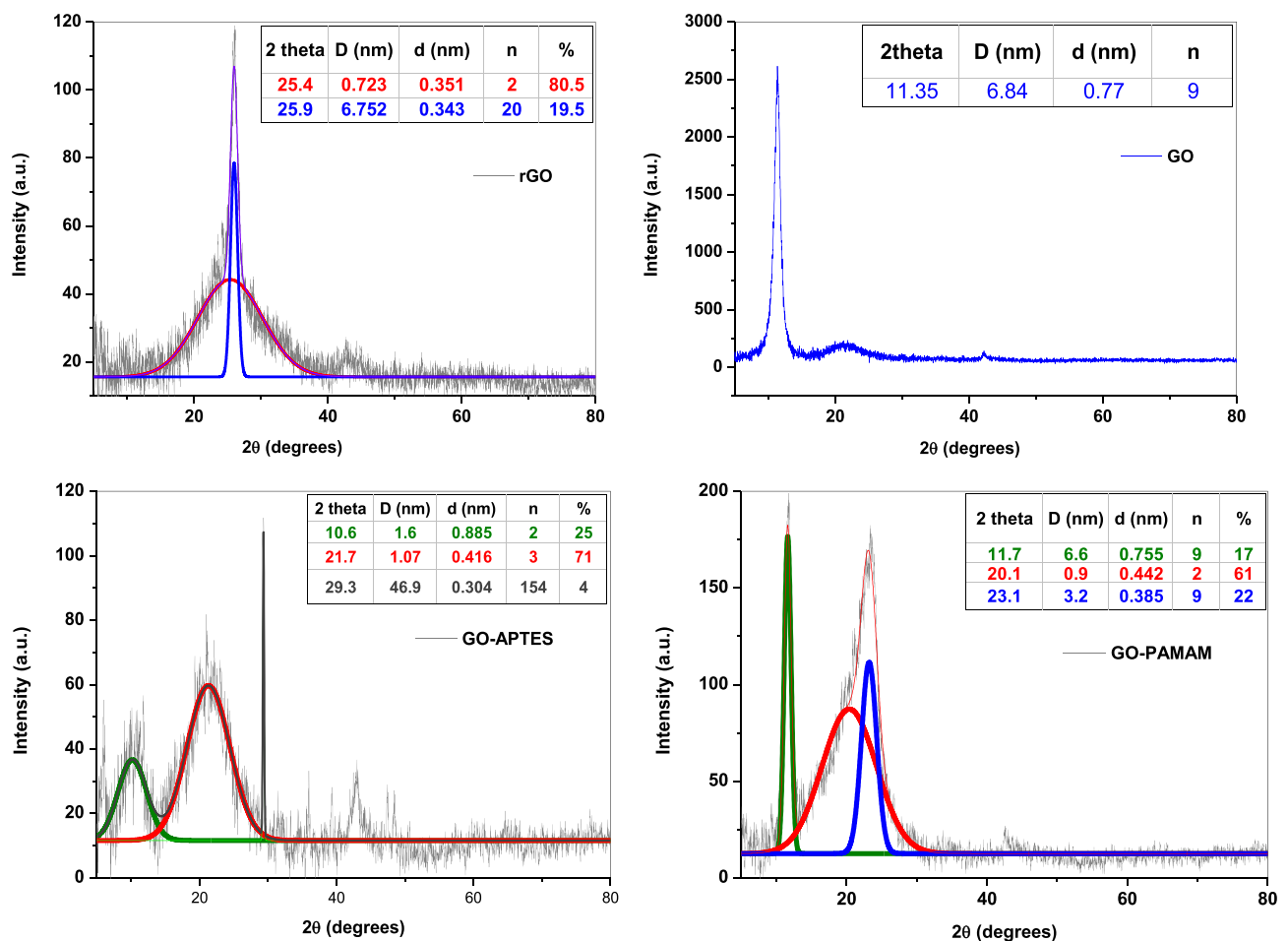
In order to assess the degree of structural disorder in the graphene nanosheet samples, Raman spectra were recorded (Fig. 4). Three important bands can be seen in these spectra: the network defect band (D) from  $1350 \text{ cm}^{-1}$ , the

characteristic graphitic band (G) located at  $1577 \text{ cm}^{-1}$ , and the 2D band located at  $2700 \text{ cm}^{-1}$  [25].

The  $I_D/I_G$  ratio can be related to the in-plane crystallite size ( $L_a$ ), indicating the defect-free domains in the graphene samples (Eq. 2) [26]:

$$L_a(\text{nm}) = \frac{560}{E_l^4} \left( \frac{I_D}{I_G} \right)^{-1} \quad (2)$$

where the laser excitation energy's equivalent is  $E_l$  (2.33 eV) and  $I_D/I_G$  is the ratio between the intensity of G and D bands [27]. The  $I_D/I_G$  ratios for rGO, GO, GO-APTES, and GO-PAMAM were 0.54, 1.1, 0.89, and 1.84 respectively as

**Fig. 5** XRD patterns and structural parameters of rGO, GO, GO-APTES, and GO-PAMAM

shown in Table 1. The increase in  $I_D/I_G$  ratio in the GO-PAMAM sample demonstrates the defect in graphene sheet caused by the graphene oxide functionalization that might induce considerable changes in the physico-chemical, structural and electrical properties. This result shows that the functionalization of GO with PAMAM alters the structure of GO through the formation of more  $sp^3$  carbon within the  $sp^2$  carbon network of graphene [28], resulting in higher  $I_D/I_G$  in the composites. The value of  $I_D/I_G$  of GO-APTES that is close to that of the unmodified GO indicates that grafting of amine molecules took place on the oxygen functional groups on the surface without disturbing the defective  $sp^3$ -hybridized sites in the basal planes of GO [29].  $L_a$  value for GO sample is about 17 nm and for rGO sample 35 nm, respectively confirming a higher oxidation degree of the GO and a much lower electrical conductivity. The  $L_a$  value for the GO-APTES sample is about 21 nm. The GO-PAMAM sample has a value of 10 nm, possessing the highest oxidation degree and the lowest electrical conductivity.

### XRD analysis

Three types of structural information determined from X-ray diffractograms were the number of graphene layers ( $n$ ), the interlayer distance ( $d$ ), and the average crystallite size ( $D$ ). The mean crystallites size ( $D$ ) was calculated from the full width at half maximum (FWHM) of the XRD peak, after instrumental broadening correction, using the Debye–Scherrer equation [30]:

$$D = \frac{K\lambda}{\beta \cos\theta} \quad (3)$$

where  $D$  is the crystallite size,  $K$  is a numerical factor commonly referred to as the crystallite-shape factor (0.9),  $\lambda$  is

**Table 2** OCP values for various Zn samples coated with  $SiO_2$  by sol-gel method

OCP (V vs. Ag/AgCl/KCl <sub>sat</sub> )		
Zn – 0.983		
Coated samples	Without sol-ageing	With 4 weeks sol-ageing
Zn/SiO <sub>2</sub>	–0.948	–0.958
Zn/SiO <sub>2</sub> -rGO	–0.947	–0.951
Zn/SiO <sub>2</sub> -GO	–0.957	–0.917
Zn/SiO <sub>2</sub> -GO-APTES	–0.957	–0.927
Zn/SiO <sub>2</sub> -GO-PAMAM	–0.961	–0.902

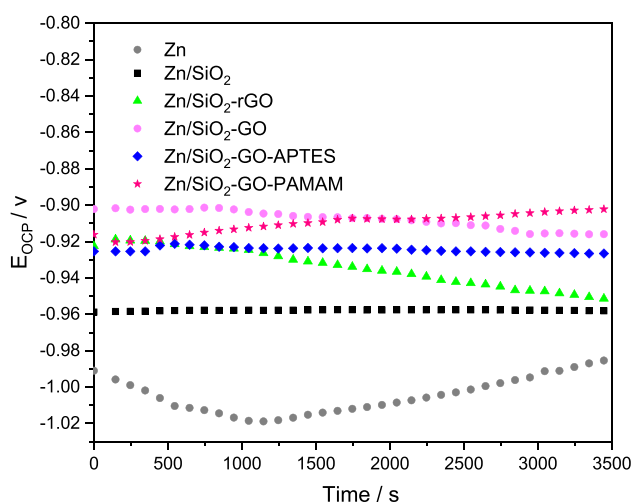
the wavelength of the X-rays,  $\beta$  is the full-width at half-maximum of the X-ray diffraction peak in radians, and  $\theta$  is the Bragg angle.

The spacing between the graphene layers ( $d$ ) was calculated with the Bragg equation [31]:

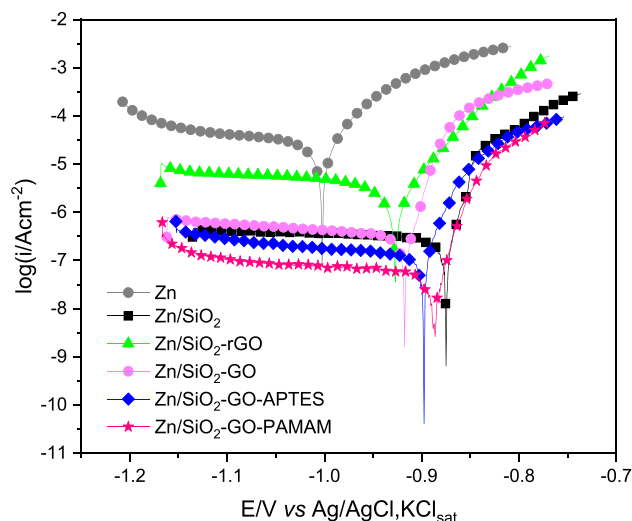
$$2d \cdot \sin\theta = n \cdot \lambda \quad (4)$$

where  $n = 1, 2, 3, \dots$  is the interference order and is an integer number,  $d$  is the distance between two layers,  $\lambda$  is the wavelength of the X-ray beam (0.154 nm), and  $\theta$  is the diffraction angle.

The number of layers was calculated from the ratio  $n = D/d$ . The amount (%) of each type of graphene was determined from XRD, expressed as the ratio of the fitted peak area to the total area of the diffractogram. The peaks close to  $24^\circ$  were asymmetric and displayed two components that were separated by fitting the XRD pattern into two theoretical Gaussian peaks (Fig. 5). The structural parameters for



**Fig. 6** OCP values and their evolution in time for Zn samples coated with different  $SiO_2$  layers from a sol aged for 4 weeks. Electrolyte, 0.2 g/L  $Na_2SO_4$  (pH 5)



**Fig. 7** Potentiodynamic polarization curves for bare and coated Zn, recorded in  $Na_2SO_4$  solution (pH 5). Scan rate, 1 mV/min. Starting potential, –250 mV vs. OCP



**Table 3** Electrochemical parameters for corrosion of Zn and different Zn/SiO<sub>2</sub> samples immersed in 0.2 g/L Na<sub>2</sub>SO<sub>4</sub> solution (pH 5)

Sample	$E_{\text{corr}}$ (mV vs. Ag/AgCl/KCl <sub>sat</sub> )	$i_{\text{corr}}$ ( $\mu\text{A}/\text{cm}^2$ )	$b_a$ (mV/dec)	$b_c$ (mV/dec)
Zn	−1002.1	42.20	65.08	57.91
Zn/SiO <sub>2</sub>	−869.8	1.14	28.82	-
Zn/SiO <sub>2</sub> -GO	−917.3	0.56	18.87	-
Zn/SiO <sub>2</sub> -rGO	−927	4.27	52.94	-
Zn/SiO <sub>2</sub> -GO-APTES	−897.4	0.17	20.69	-
Zn/SiO <sub>2</sub> -GO-PAMAM	−886.2	0.09	24.02	-

the samples, calculated from XRD data, are presented in the inset of Fig. 5.

Figure 5 also shows the XRD patterns of GO-APTES and GO-PAMAM nanoparticles. We observed the main peaks at  $2\theta = 10.63^\circ$ ,  $21.78^\circ$ , and  $29.37^\circ$  for GO-APTES and at  $2\theta = 11.74^\circ$  and  $23.46^\circ$  for GO-PAMAM. The peaks at  $10.63^\circ$  (GO-APTES) and  $11.74^\circ$  (GO-PAMAM) can be attributed to the unreacted GO. The pointed sharp peaks reflect a certain amount of crystallinity of GO-APTES and GO-PAMAM nanomaterials. In the GO-APTES sample, a small percentage of graphite (4%) appears.

### Electrochemical measurements

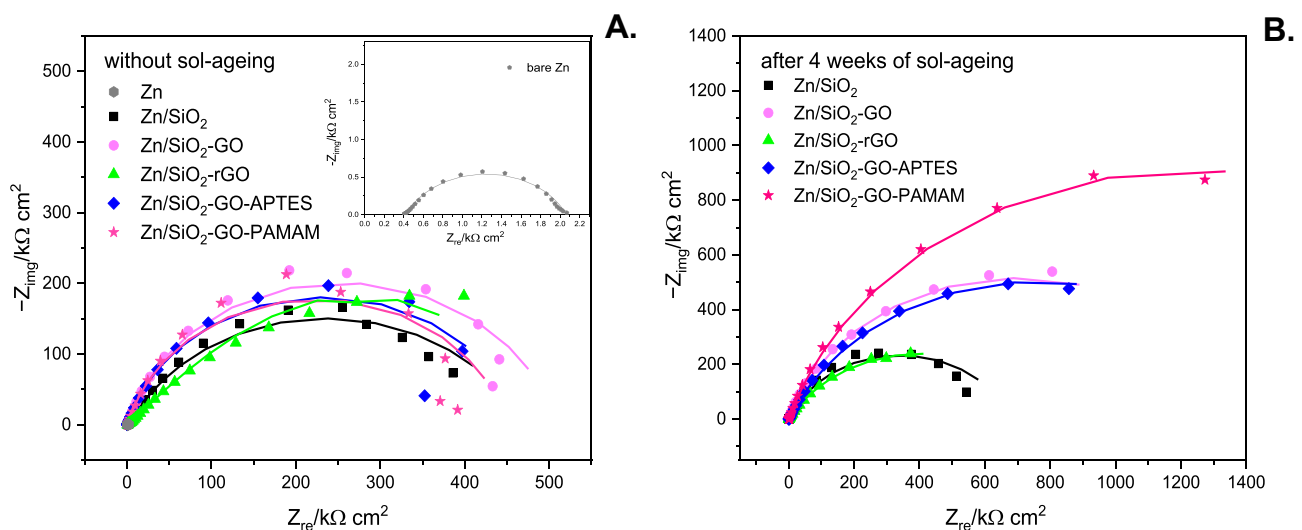
The OCP values and their evolution in time for bare Zn and the different coated samples immersed in Na<sub>2</sub>SO<sub>4</sub> solution (pH 5) are presented in Fig. 6. It can be observed that after 1 h, the OCP values of Zn coated with different silica layers were shifted toward more positive potentials as compared to bare Zn. In other words, an ennoblement of the surface was noticed. However, the magnitude of the positive shift of the corrosion potential is different for various coatings.

After 1 h, the most positive OCP is noticed for the GO-PAMAM containing coating prepared from a sol aged for 4 weeks. This can be attributed mainly to a braking of the anodic reaction due to a better protection of zinc conferred by these coatings.

The values for OCP of the Zn samples prepared by sol–gel method without or with 4 weeks sol-ageing are presented in Table 2.

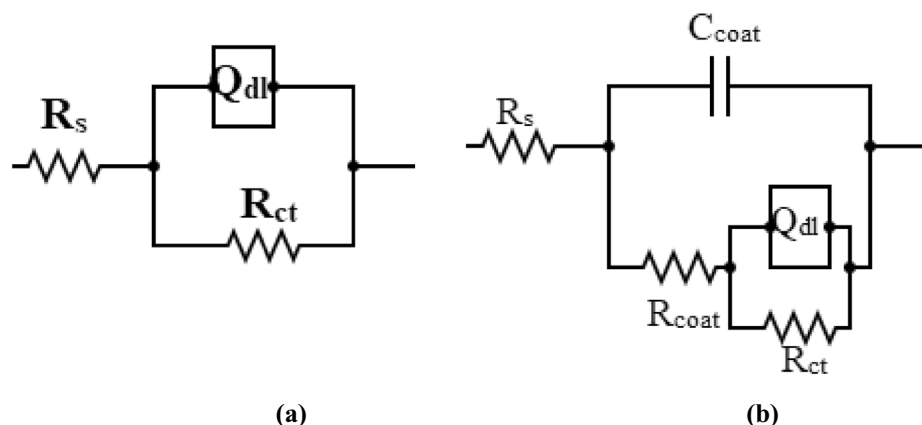
In order to get a deeper insight into the anti-corrosion protection mechanism of zinc, coated with different types of layers, EIS measurements were performed.

EIS is based on two hypotheses: linearity of the  $I$  vs.  $E$  curve and stationarity. True behavior of electrode in term of corresponding resistances should be deduced only at steady-state position (i.e. OCP), where the measurements reflect the original characteristics of electrode–electrolyte system. The potentiodynamic measurements start far from a steady-state and may be a source of error. A linear polarization record starts at a potential about  $-250$  mV lower than OCP. Moreover, determination of  $E_{\text{corr}}$  from the polarization curves is subjected to a number of parameters, i.e., applied potential, current acquisition, time of the polarization test,



**Fig. 8** Nyquist plots of silica and modified-silica coatings without (A) and after 4 weeks (B) of sol-ageing immersed in 0.2 g/L Na<sub>2</sub>SO<sub>4</sub> solution (pH=5.0); the solid lines are the fitting results; the impedance values were normalized with respect to total surface area (2 cm<sup>2</sup>)

**Fig. 9** Electric equivalent circuits used for fitting the impedance spectra for bare Zn (a) and coated Zn samples (b)



IR drop due to the ionic solution resistance, and so on. This is why investigation of the system by means of electrochemical impedance spectroscopy is more trustworthy.

Nevertheless, potentiodynamic polarization curves (Fig. 7) confirmed the tendency of  $E_{\text{corr}}$  to shift toward more positive values and suggest a mixed mechanism of inhibition for all  $\text{SiO}_2$  coatings, as both branches (anodic and cathodic) of the semilogarithmic curves were shifted toward lower current densities. The kinetic parameters extracted from these curves by using Tafel interpretation are presented in Table 3. Due to diffusion limitation of the cathodic reaction (oxygen reduction), the cathodic Tafel coefficient,  $b_c$ , could not be used for  $i_{\text{corr}}$  calculation. The most resistant coating seemed to be Zn/ $\text{SiO}_2$ -GO-PAMAM, followed closely by Zn/ $\text{SiO}_2$ -GO-APTES.

Even if the polarization curves give some useful information related to the corrosion kinetics, as already mentioned above, impedance measurements are more reliable in what the investigation of coated metals' behaviour is concerned. This is the reason for which more attention was ascribed to EIS measurements carried out for various Zn/ $\text{SiO}_2$  systems, at OCP, and the results are presented in what follows.

Because the polycondensation step occurring during the preparation of coatings by the sol–gel method has relatively low kinetics, it was of interest to examine the role of sol-aging on the performances of the coatings. The impedance

spectra of all investigated coatings without and after sol-aging are presented in Fig. 8.

Further, impedance data were modelled using the electrical circuits presented in Fig. 9. With the scope of determining the accuracy of the fitting for all of the previously presented cases, the latter was estimated with the relative standard error percent calculated for the equivalent circuit parameters (mostly below 10%), respectively the chi-squared  $\chi^2$  value (around  $10^{-3}$ ).

In case of bare Zn, the electrical equivalent circuit is composed only of the solution resistance, a constant phase element simulating the double layer capacitance, and a charge transfer resistance in parallel  $R_s(Q_{dl}R_{ct})$  (Fig. 9a). The electrical circuit in the case of coated samples consists of a resistor  $R_s$ , corresponding to the solution resistance, a resistor  $R_{\text{coat}}$  and a capacitor  $C_{\text{coat}}$  in parallel, which represents the coating resistance and its related capacitance, respectively, and lastly, a parallel combination of the charge transfer resistance  $R_{ct}$  and a constant phase element, simulating to the double-layer capacitance at the metal/solution interface ( $Q_{dl}$ ) (Fig. 9b).

The constant phase element ( $Q$ , CPE) was used instead of capacitance to describe the non-ideal capacitive behaviour of the double layer. The origins of CPE behavior are numerous and some of them quite complex. The existence of CPE indicates that some property of the system

**Table 4** Electrochemical parameter values for Zn/ $\text{SiO}_2$  and  $\text{SiO}_2$  modified GO coated samples without sol-aging, immersed in 0.2 g/L  $\text{Na}_2\text{SO}_4$  solution (pH=5.0) obtained from the fitting of the equivalent electrical circuit from Fig. 9 ( $n \sim 0.8$ )

Samples without sol-aging	$R_s$ ( $\text{k}\Omega \text{ cm}^2$ )	$C_{\text{coat}}$ ( $\mu\text{F}/\text{cm}^2$ )	$R_{\text{coat}}$ ( $\text{k}\Omega \text{ cm}^2$ )	$Q_{dl}$ ( $\mu\text{Ss}^n/\text{cm}^2$ )	$R_{ct}$ ( $\text{k}\Omega \text{ cm}^2$ )	$R_p = R_{\text{coat}} + R_{ct}$ ( $\text{k}\Omega \text{ cm}^2$ )	$\chi^2$
Zn	0.42	-	-	104.30	2	2.00	$8.05 \times 10^{-4}$
Zn/ $\text{SiO}_2$	0.58	0.08	2.37	3.89	468	470.37	$7.12 \times 10^{-3}$
Zn/ $\text{SiO}_2$ -GO	0.59	0.10	0.47	3.60	507	507.47	$3.38 \times 10^{-3}$
Zn/ $\text{SiO}_2$ -rGO	0.91	0.09	3.35	6.17	727	730.35	$5.52 \times 10^{-3}$
Zn/ $\text{SiO}_2$ -GO-APTES	0.34	0.23	0.14	6.53	465	465.14	$4.84 \times 10^{-3}$
Zn/ $\text{SiO}_2$ -GO-PAMAM	0.71	0.17	0.47	3.72	449	449.47	$7.76 \times 10^{-3}$

**Table 5** Electrochemical parameter values for Zn/SiO<sub>2</sub> and SiO<sub>2</sub> graphene-coated samples after 4 weeks of sol-ageing, immersed in 0.2 g/L Na<sub>2</sub>SO<sub>4</sub> solution (pH=5.0) calculated by non-linear regression of the impedance data using the equivalent electrical circuit from Fig. 7 ( $n \sim 0.8$ )

Samples after 4-week sol-ageing	$R_s$ (k $\Omega$ cm <sup>2</sup> )	$C_{\text{coat}}$ ( $\mu$ F/cm <sup>2</sup> )	$R_{\text{coat}}$ (k $\Omega$ cm <sup>2</sup> )	$Q_{dl}$ ( $\mu$ Ss <sup><math>n</math></sup> /cm <sup>2</sup> )	$R_{ct}$ (k $\Omega$ cm <sup>2</sup> )	$R_p = R_{\text{coat}} + R_{ct}$ (k $\Omega$ cm <sup>2</sup> )	$\chi^2$
Zn/SiO <sub>2</sub>	0.56	0.09	2.06	3.56	678	680.06	$8.46 \times 10^{-3}$
Zn/SiO <sub>2</sub> -GO	0.28	0.29	0.18	4.37	1407	1407.18	$3.15 \times 10^{-3}$
Zn/SiO <sub>2</sub> -rGO	0.17	0.03	0.15	7.87	806	806.15	$1.74 \times 10^{-3}$
Zn/SiO <sub>2</sub> -GO-APTES	0.53	0.17	0.41	3.97	1527	1527.41	$2.61 \times 10^{-3}$
Zn/SiO <sub>2</sub> -GO-PAMAM	0.60	0.29	0.63	3.12	2488	2488.63	$3.14 \times 10^{-3}$

is not homogeneous, or that there is a distribution of the values of some physical properties of the system. Possible parameters that are at the origin of CPE in case of corrosion of coated zinc are the substrate's surface roughness, an inhomogeneity of reaction rates on the surface, varying thickness or composition of the coating, a non-uniform current distribution, etc.

Table 4 contains the corresponding parameters obtained from the fitting of the equivalent electrical circuits from Fig. 9 to the experimental diagrams for the samples without sol-ageing, and Table 5, the electrochemical parameter values of the coated zinc samples prepared after 4 weeks of sol-ageing. In all cases of doped silica coatings, the results were better than in the absence of GO-based dopants (higher  $R_p$ ).

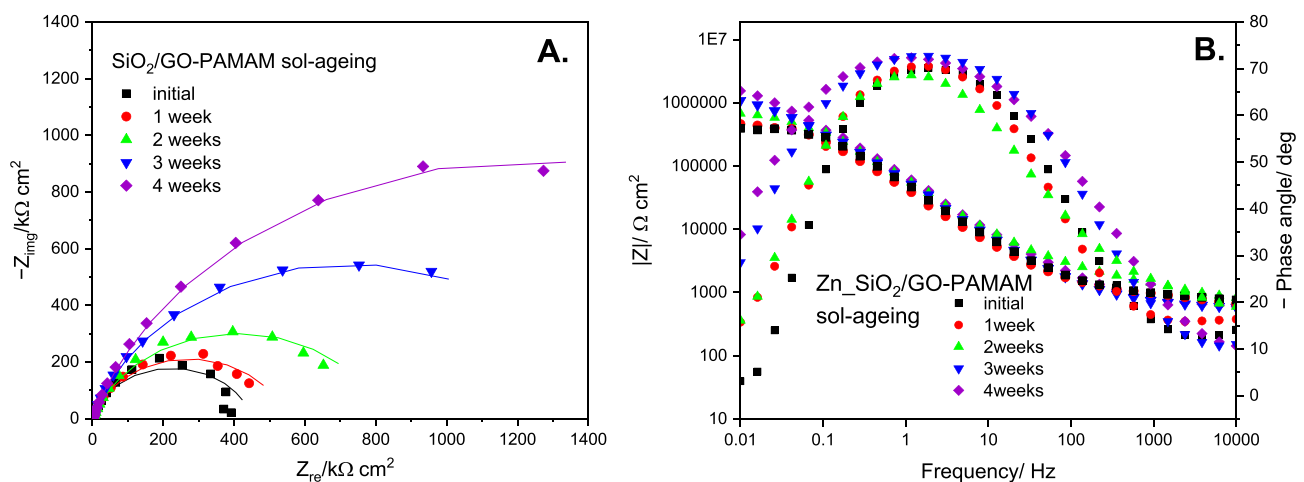
Another observation is that after the sol is aged for 4 weeks, an increase in the  $R_p$  values occur in the case of every coating, the increase being less significant in the case of SiO<sub>2</sub> and SiO<sub>2</sub>-rGO coatings. This phenomenon can be explained by the evolution of the polycondensation reaction that occurs inside the silica sol during 4 weeks.

The most spectacular change is observed in the case of SiO<sub>2</sub>-GO-PAMAM coatings (Fig. 8; Table 5).  $R_{ct}$ , which

decides the barrier properties of the coatings, represents the biggest contribution to the polarization resistance ( $R_p$ ). The SiO<sub>2</sub>-GO-PAMAM coating owns the highest  $R_p$  value of 2488.63 k $\Omega$  cm<sup>2</sup>, followed by the GO-APTES silica composite coating and GO containing silica layers.

This could be explained by the compatibility of the nano-fillers with the silica matrix, that requires hydroxyl groups, which can be found on the surface of the GO sheets. This way, the hydroxyl groups could undergo condensation reaction on the neighbouring silane molecules [32]. When modified with PAMAM, the GO conserves its (-OH) groups on the surface, as we could observe from the FT-IR results (Fig. 1), leading to a better incorporation of the filler in the silica matrix. On the other hand, the higher corrosion protection properties of the Zn/SiO<sub>2</sub>-GO-PAMAM composite coatings can be also attributed to the dendrimer's intrinsic corrosion inhibiting effect [33].

After calculating the inhibition efficiency (IE%) from the  $R_p$  values, all the IE% values are above 99.7%, the SiO<sub>2</sub> coatings offering a great protection to the Zn substrate. The values are high, because  $R_p$  for the bare Zn is negligible

**Fig. 10** Nyquist (A) and Bode impedance spectra with phase angle plots (B) for SiO<sub>2</sub>-GO-PAMAM coatings prepared with different sol-ageing duration, immersed in 0.2 g/L Na<sub>2</sub>SO<sub>4</sub> solution (pH=5.0); the

solid lines represent the fitting results, and the impedance values were normalized with respect to total surface area (2 cm<sup>2</sup>)

**Table 6** Electrochemical parameter values for SiO<sub>2</sub>-GO-PAMAM-coated samples differentiated by ageing the sol, calculated by non-linear regression of the impedance data using the equivalent electrical circuit from above ( $n \sim 0.8$ )

Sol-ageing duration	$R_s$ (k $\Omega$ cm <sup>2</sup> )	$C_{\text{coat}}$ ( $\mu$ F/cm <sup>2</sup> )	$R_{\text{coat}}$ (k $\Omega$ cm <sup>2</sup> )	$Q_{dl}$ ( $\mu$ Ss <sup>0.8</sup> /cm <sup>2</sup> )	$R_{ct}$ (k $\Omega$ cm <sup>2</sup> )	$R_p = R_{\text{coat}} + R_{ct}$ (k $\Omega$ cm <sup>2</sup> )	$\chi^2$
Initial	0.71	0.17	0.47	3.71	449	449.47	$7.76 \times 10^{-3}$
1 week	0.61	0.14	0.52	4.86	545	545.52	$4.57 \times 10^{-3}$
2 weeks	0.81	0.12	1.26	3.53	820	821.26	$7.61 \times 10^{-3}$
3 weeks	0.55	0.24	0.31	3.72	1457	1457.31	$3.29 \times 10^{-3}$
4 weeks	0.60	0.29	0.63	3.12	2488	2488.63	$3.14 \times 10^{-3}$

compared to the  $R_p$  of the coatings dipped from the sols aged for 4 weeks.

The evolution of Nyquist and Bode impedance diagrams recorded in 0.2 g/L Na<sub>2</sub>SO<sub>4</sub> solution (pH = 5.0) as a function of the duration of sol-ageing in the coatings' preparation step is depicted in Fig. 10.

The phase angle of around  $-70^\circ$  suggests that the coatings have a predominant capacitive behaviour. A phase angle of  $0^\circ$  corresponds to an ideal resistor,  $+90^\circ$  corresponds to an ideal inductor, and  $-90^\circ$  corresponds to an ideal capacitor. Values in between may indicate non-ideal, mixed behaviour, depending on the system under study. Furthermore, the single time constant Bode curves suggest that the electrolyte penetrated the coating, but did not reach the zinc/coating interface [34].

The electrochemical parameter values for SiO<sub>2</sub>-GO-PAMAM coated samples differentiated by ageing the sol are presented in Table 6.

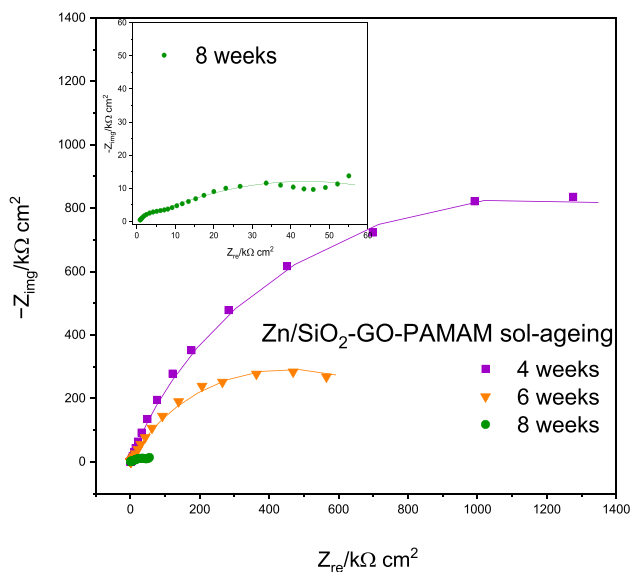
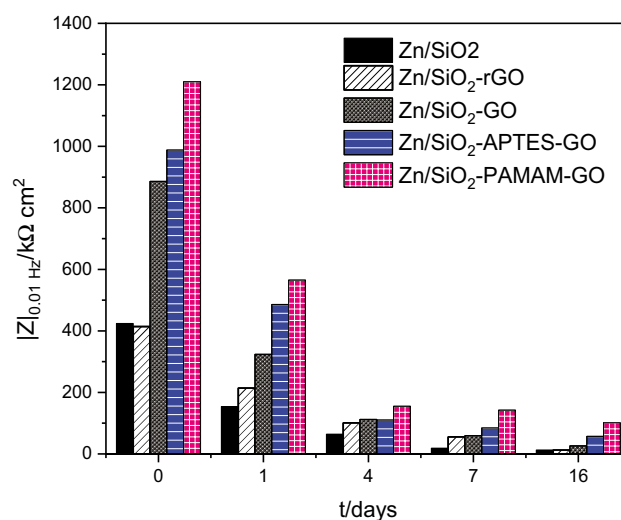
From Fig. 10 can be observed that, on the second week, the coating's  $R_p$  value almost doubled compared to the

sample coated from the initial precursor sol. After 4 weeks the polarization resistance reaches 2488 k $\Omega$  cm<sup>2</sup> from the 449 k $\Omega$  cm<sup>2</sup> start value.

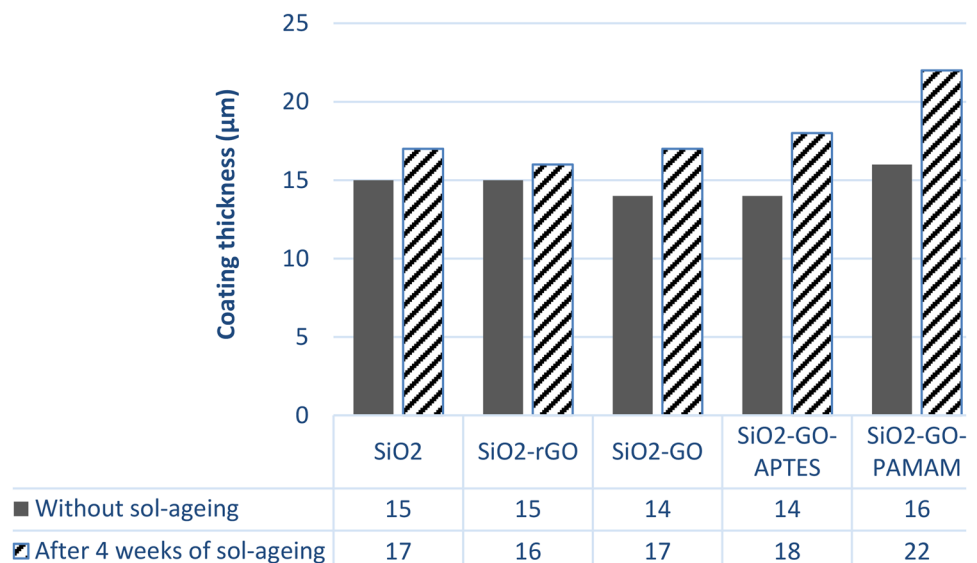
In the Bode plot of modulus of impedance vs. frequency (Fig. 10B), the impedance value determined at 0.01 Hz was chosen as the parameter representing the corrosion resistance of the coating. It can be observed that with sol-ageing the  $|Z|_{0.01 \text{ Hz}}$  parameter for SiO<sub>2</sub>-GO-PAMAM increases systematically until week 4.

Continuing the experiments with a sol-ageing period greater than 4 weeks, the situation changes dramatically. The impedance decreases significantly after 6 weeks and the value recorded after 8 weeks (Fig. 11) is much smaller even than that of the undoped silica coating.

It can be observed that after reaching a maximum, the coating's anti-corrosive properties decrease, which can be explained by the occurrence of a relative brittleness of the coating. It is visible, that at 8 weeks sol-ageing, the coating begins to peel off from the substrate leading to the decline of the coating's protection performance. The protective properties of the films deteriorate when the sol gets closer to the gel point. It is assumed that close to this point, the sol begins to form aggregates, so the coated

**Fig. 11** Evolution of Nyquist impedance plots of SiO<sub>2</sub>-GO-PAMAM coatings prepared with 4, 6, and 8 weeks of sol-ageing when immersed in 0.2 g/L Na<sub>2</sub>SO<sub>4</sub> solution (pH = 5.0); the fitting results are represented with solid lines; the impedance values were normalized with respect to total surface area (2 cm<sup>2</sup>)**Fig. 12**  $|Z|_{0.01 \text{ Hz}}$  variation in time for the silica-based coatings

**Fig. 13** The thickness of the silica coatings and of the composite coatings containing nanofillers, with or without sol-ageing



layers are not homogeneous anymore, and prone to cracking [35]. This effect is present in the case of each silica sol, but the time when this happens differs.

Concluding, the optimal duration for the sol-ageing is 4 weeks.

### Influence of immersion time

The behaviour of the coated samples immersed in a 0.2-g/L Na<sub>2</sub>SO<sub>4</sub> solution (pH 5) was investigated in a large time range. It can be seen from Fig. 12 that at the moment of immersion the  $|Z|_{0.01 \text{ Hz}}$  values for all coated systems are greater than that for SiO<sub>2</sub> samples and by increasing the immersion time the  $|Z|_{0.01 \text{ Hz}}$  value significantly decreased, indicating the protection of the coating performance decline. Thus, the decrease in  $|Z|_{0.01 \text{ Hz}}$  at long immersion time is assigned to the electrolyte diffusion into the coating matrix, which results in the coating deterioration, the coating delaminated area progress, and barrier properties alteration [36]. The electrolyte diffusion into the coating/metal interface caused the zinc-silica interfacial adhesion bond destruction and, consequently, under-film corrosion.

Nevertheless, the most resistant seems to be same SiO<sub>2</sub>-GO-PAMAM-coated zinc samples. It becomes clear that PAMAM improves the dispersion of GO in the SiO<sub>2</sub> matrix. Moreover, because of GO-PAMAM nanosheets high specific surface area and impermeability against water and


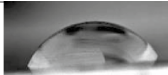


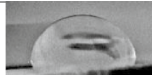
ions, the pathway of the electrolyte was lengthened. The interfacial adhesion improvement is mainly responsible for this behaviour. On the surface of GO sheets, the appearance of the polar amino groups from the PAMAM molecules leads to interaction with the oxide layer formed on the metal surface, which provides strong adhesion bonds and silica/zinc interfacial bonds strength improvement [37].

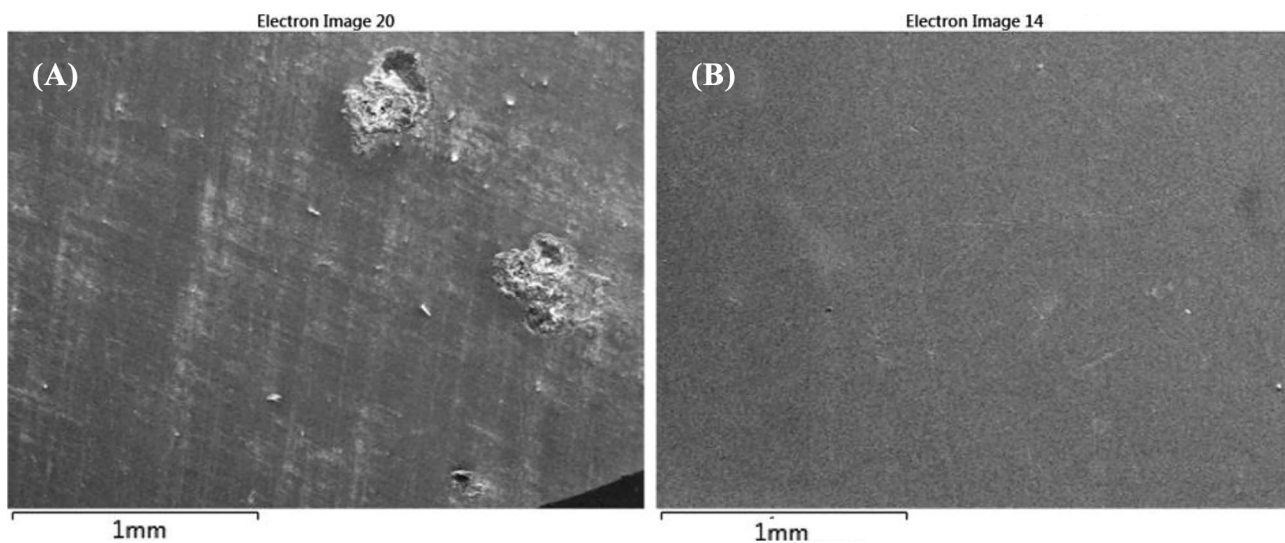
The compatibility of the nanosheets with the silica matrix requires -OH groups. In the case of GO modified with PAMAM, the -OH groups remain on the surface of the GO. Moreover, the in-plane crystallite size ( $L_a$ ) calculated from Raman measurements (Table 1) prove that the GO-PAMAM nanoparticles have the highest oxidation degree. As can be seen from Fig. 5, 61% of GO-PAMAM powder is represented by particles of 0.9 nm. These small dimensions help their uniform distribution in the coatings, excluding agglomerates which can offer a shortcut for the penetration of corrosive molecules [32].

### Coating thickness and contact angle measurements

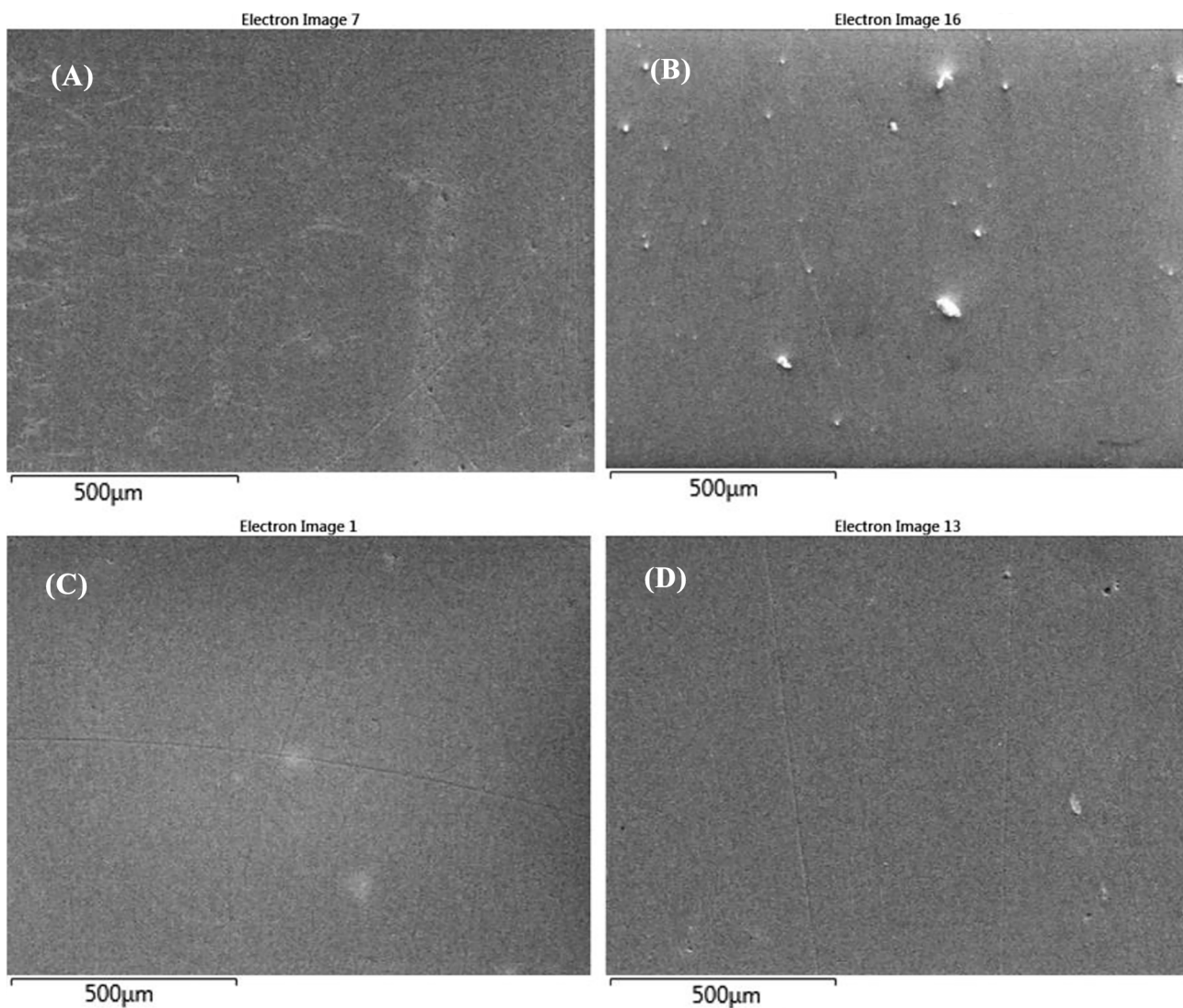
As expected, the thickness of silica layers depend on the duration of sol-ageing process. As we can observe in Fig. 13, in case of silica coatings and silica containing rGO, this process has an insignificant effect, the thickness value remaining at around 17 µm, and 16 µm, respectively. With the incorporation

**Table 7** Variation of contact angles of electrolyte droplets deposited on silica-based surfaces

Coating	Zn/SiO <sub>2</sub>	Zn/SiO <sub>2</sub> -rGO	Zn/SiO <sub>2</sub> -GO-APTES	Zn/SiO <sub>2</sub> -GO	Zn/SiO <sub>2</sub> -GO-PAMAM
					
Contact angle	65°	62°	72°	81°	82°



**Fig. 14** SEM images of SiO<sub>2</sub> coating (A) and Zn/SiO<sub>2</sub>-GO-PAMAM coating (B) after 2 weeks immersion in 0.2 g/L Na<sub>2</sub>SO<sub>4</sub> (pH 5)



**Fig. 15** SEM images of Zn/SiO<sub>2</sub>-GO-PAMAM coating from initial sol (A), and from sol aged during 4 weeks (C), left 2 weeks at ambient temperature at air; Zn/SiO<sub>2</sub>-GO-PAMAM coating from initial sol (B),

and from sol aged during 4 weeks (D), immersed in 0.2 g/L Na<sub>2</sub>SO<sub>4</sub> (pH 5) for 2 weeks

of different GO nanofillers, the coatings prepared from the sol without ageing have a thickness of ~14–16  $\mu\text{m}$ , but after 4 weeks of sol-ageing, thanks to the polycondensation reaction that occurs inside the silica sol and the supposed increase in density of the sol, the coating thickness increases to even 22  $\mu\text{m}$  in case of  $\text{SiO}_2$ -GO-PAMAM composite coatings.

The wettability of the composite silica coatings was investigated by the sessile drop method. For this purpose, electrolyte droplets were formed on the dry layers and their characteristics were measured. The images of the corresponding droplets are presented in Table 7.

The  $\text{SiO}_2$  coating has a hydrophilic nature due to the remained untransformed hydroxyl groups at its surface after annealing at 150  $^\circ\text{C}$  [38]. The density of the aforementioned groups is reduced through the interaction with the functional groups of the GO (hydroxyl, carbonyl, carboxyl, epoxy) added to the silica matrix causing the increased contact angle in comparison with undoped silica. The addition of APTES and PAMAM modifying agents to GO can change the amount of its functional groups, by engaging in bond forming, that can react with the silicas' hydroxyl groups. This could be a possible explanation for the wettability modification of modified-GO-silica coatings. In the case of  $\text{SiO}_2$ -GO-APTES can be assumed a higher density of hydrophile groups that is responsible for the lower contact angle in comparison with  $\text{SiO}_2$ -GO. The PAMAM dendrimer due to the group's higher size/volume and its steric effect can block the access to the hydrophile functional groups making the coating less wettable. In the case of the rGO, the amount of oxygen containing functional groups is lower, therefore the bond formation with the -OH groups of the silica matrix is diminished too, so their hydrophilic effect is retained.

### Scanning electron microscopy measurements

SEM images were taken of the  $\text{SiO}_2$  and  $\text{SiO}_2$ /GO-PAMAM coatings after immersion in 0.2 g/L  $\text{Na}_2\text{SO}_4$  electrolyte (pH 5) for 2 weeks. On the surface of  $\text{SiO}_2$  coatings after immersion in the electrolyte, the appearance of corrosion is accentuated in comparison with the  $\text{SiO}_2$  containing GO-PAMAM (Fig. 14).

The difference between the  $\text{SiO}_2$ /GO-PAMAM sample coated from the initial sol (Fig. 15A, B) and from the sol aged for 4 weeks (Fig. 15C, D) becomes visible after immersion in 0.2 g/L  $\text{Na}_2\text{SO}_4$  solution (pH 5), the sample coated from the initial sol presenting more corrosion points (Fig. 15B).

### Conclusions

Considering all the results, several conclusions can be drawn:

- In the case of PAMAM dendrimer modified GO nanosheets, FT-IR spectra confirm that a reaction takes place between

the amino groups of the dendrimer and the carboxyl groups of the GO, proving GO functionalization.

- The in-plane crystallite size ( $L_a$ ) calculated from Raman measurements proves that the GO-PAMAM nanoparticles have the highest oxidation degree and the lowest electrical conductivity.
- XRD patterns of GO-APTES and GO-PAMAM show pointed sharp peaks, reflecting a certain amount of crystallinity of these nanoparticles. 61% of GO-PAMAM powder is represented by particles of  $D=0.9$  nm (average crystallite size). These small dimensions help their uniform distribution in the coatings.
- The OCP values of Zn coated with different silica layers were shifted toward more positive potentials as compared to bare Zn, suggesting an ennoblement of the surface after coating.
- The potentiodynamic polarization curves confirmed the tendency of  $E_{\text{corr}}$  to shift toward more positive values and suggest a mixed mechanism of inhibition for all  $\text{SiO}_2$  coatings, as both branches (anodic and cathodic) of the semilogarithmic curves were shifted toward lower current densities.
- EIS measurements carried out in 0.2 g/L  $\text{Na}_2\text{SO}_4$  (pH 5) at OCP allowed estimation of the different coatings' corrosion resistance. The parameters of the corrosion process were estimated by fitting the equivalent electrical circuits to the experimental diagrams for the samples prepared without sol-ageing, and after 4 weeks of sol-ageing. In all cases of composite silica coatings, the results were better than in the absence of GO-based dopants and after 4 weeks of sol-ageing (higher  $R_p$ ), suggesting a favourable evolution of the polycondensation reaction. The incorporation of GO-PAMAM nanosheets into the silica matrix remarkably increased its barrier protection performance, leading to the most corrosion-resistant and water repellent coating among the investigated ones.
- The behaviour of the zinc-coated samples immersed in a 0.2 g/L  $\text{Na}_2\text{SO}_4$  solution (pH 5) was investigated in a large time range. At the moment of immersion, the  $|Z|_{0.01 \text{ Hz}}$  values for all coated systems are greater than that for pure  $\text{SiO}_2$  coatings. At the same time, the increase of immersion time led to a serious decrease of  $|Z|_{0.01 \text{ Hz}}$ , indicating the protection of the coating performance decline. Although, the  $\text{SiO}_2$ -GO-PAMAM coating exhibited the most favourable evolution.
- All investigation methods lead to the conclusion that  $\text{SiO}_2$  matrix modification with GO-PAMAM nanosheets significantly improved the corrosion resistance of the composite coatings, mainly by reducing the penetration of the electrolyte into the silica/zinc interface.

**Author contribution** All authors contributed to the study conception and design. Material preparation, data collection, and analysis were

performed by Tamara Ovari, Gabriella Szabo, G. Katona, and Maria Coros. The first draft of the manuscript was written by Tamara Ovari, and all authors commented on previous versions of the manuscript. The work was carried out under the supervision of Liana Maria Muresan, who elaborated the final version of the paper. All authors read and approved the final manuscript.

**Funding** The present work has received financial support through the project: Entrepreneurship for innovation through doctoral and post-doctoral research, POCU/380/6/13/123886, co-financed by the European Social Fund, through the Operational Program for Human Capital 2014–2020.

**Data availability** Authors can confirm that all relevant data are included in the article.

## Declarations

**Competing interests** The authors declare no competing interests.

## References

- Ahmadi A, Ramezanzadeh B, Mahdavian M (2016) Hybrid silane coating reinforced with silanized graphene oxide nanosheets with improved corrosion protective performance. *RSC Adv* 59:54102–54112. <https://doi.org/10.1039/C6RA04843A>
- Cotolan N, Varvara S, Albert E, Szabo G, Horvolgyi Z, Muresan L-M (2016) Evaluation of corrosion inhibition performance of silica sol-gel layers deposited on galvanised steel. *Corros Eng Sci Technol* 51:373. <https://doi.org/10.1080/1478422X.2015.1120404>
- Li Y, Wu C, Xue M, Cai J, Huang Y, Yang H (2019) Preparation of sol-gel derived anticorrosive coating on Q235 carbon steel substrate with long-term corrosion prevention durability. *Materials* 12:1960. <https://doi.org/10.3390/ma12121960>
- Xue B, Yu M, Liu J et al (2017) Corrosion protection of AA2024-T3 by sol-gel film modified with graphene oxide. *J Alloys Compd* 725:84–95. <https://doi.org/10.1016/j.jallcom.2017.05.091>
- Albert E, Cotolan N, Nagy N, Gy S, Szabó G, Muresan L, Hórvölgyi Z (2015) Mesoporous silica coatings with improved corrosion protection properties. *Microporous Mesoporous Mater* 206:102–113
- Szabo G, Albert E, Both J, Kocs L, Gy S, Szoke A, Horvolgyi Z, Muresan LM (2019) Influence of embedded inhibitors on the corrosion resistance of zinc coated with mesoporous silica layers. *Surf Interfaces* 15:216–223. <https://doi.org/10.1016/j.surfifin.2019.03.007>
- Pourhashem S, Vaezi MR, Rashidi A et al (2017) Distinctive roles of silane coupling agents on the corrosion inhibition performance of graphene oxide in epoxy coating. *Prog Org Coat* 111:47–56. <https://doi.org/10.1016/j.porgcoat.2017.05.008>
- Ramezanzadeh B, Niroumandrad S, Ahmadi A et al (2016) Enhancement of barrier and corrosion protection performance of an epoxy coating through wet transfer of amino functionalized graphene oxide. *Corros Sci* 103:283–304. <https://doi.org/10.1016/j.corsci.2015.11.033>
- Ding R, Li W, Wang X et al (2018) A brief review of corrosion protective films and coatings on graphene and graphene oxide. *J Alloys Compd* 764:1039–1055. <https://doi.org/10.1016/j.jallcom.2018.06.133>
- Nonahal M, Rastin H, Saeb MR et al (2018) Epoxy/PAMAM dendrimer-modified graphene oxide nanocomposite coatings. Nonisothermal cure kinetics study. *Prog Org Coat* 114:233–243. <https://doi.org/10.1016/j.porgcoat.2017.10.023>
- Kuila T, Bose S, Mishra AK et al (2012) Chemical functionalization of graphene and its applications. *Prog Mater Sci* 57:1061–1105. <https://doi.org/10.1016/j.pmatsci.2012.03.002>
- Wang H, He Y, Fei G et al (2019) Functionalizing graphene with titanate coupling agents as reinforcement for one-component waterborne poly(urethane-acrylate) anticorrosion coatings. *Chem Eng J* 359:331–343. <https://doi.org/10.1016/j.cej.2018.11.133>
- Othman NR, Yahya WZN, Ismail MC et al (2020) Highly dispersed graphene oxide–zinc oxide nanohybrids in epoxy coating with improved water barrier properties and corrosion resistance. *J Coat Technol Res* 17:101–114. <https://doi.org/10.1007/s11998-019-00245-y>
- Yu Z, Di H, Ma Y et al (2015) Preparation of graphene oxide modified by titanium dioxide to enhance the anti-corrosion performance of epoxy coatings. *Surf Coat Technol* 276:471–478. <https://doi.org/10.1016/j.surfcoat.2015.06.027>
- Yu Z, Lv L, Ma Y et al (2016) Covalent modification of graphene oxide by metronidazole for reinforced anti-corrosion properties of epoxy coatings. *RSC Adv* 6:18217–18226. <https://doi.org/10.1039/C5RA23595B>
- Hosseinpour A, Abadchi MR, Mirzaee M et al (2021) Recent advances and future perspectives for carbon nanostructures reinforced organic coating for anti-corrosion application. *Surf Interfaces* 23:100994. <https://doi.org/10.1016/j.surfint.2021.100994>
- Parhizkar N, Ramezanzadeh B, Shahrabi T (2018) Corrosion protection and adhesion properties of the epoxy coating applied on the steel substrate pre-treated by a sol-gel based silane coating filled with amino and isocyanate silane functionalized graphene oxide nanosheets. *Appl Surf Sci* 439:45–59. <https://doi.org/10.1016/j.apsusc.2017.12.240>
- Gholipour-Mahmoudalilou M, Roghani-Mamaqani H, Azimi R et al (2018) Preparation of hyperbranched poly (amidoamine)-grafted graphene nanolayers as a composite and curing agent for epoxy resin. *Appl Surf Sci* 428:1061–1069. <https://doi.org/10.1016/j.apsusc.2017.09.237>
- Pogacean F, Socaci C, Pruneanu S et al (2015) Graphene based nanomaterials as chemical sensors for hydrogen peroxide—a comparison study of their intrinsic peroxidase catalytic behavior. *Sens Actuators B Chem* 213:474–483. <https://doi.org/10.1016/j.snb.2015.02.124>
- Pruneanu S, Biris AR, Pogacean F et al (2015) The influence of uric and ascorbic acid on the electrochemical detection of dopamine using graphene-modified electrodes. *Electrochim Acta* 154:197–204. <https://doi.org/10.1016/j.electacta.2014.12.046>
- Ovári TR, Katona G, Szabó G et al (2022) Electrochemical evaluation of the relationship between the thermal treatment and the protective properties of thin silica coatings on zinc substrates. *Studia UBB Chemia* 67:227–243. <https://doi.org/10.24193/subbchem.2022.1.15>
- Ramos-Galicia L, Mendez LN, Martínez-Hernández AL et al (2013) Improved performance of an epoxy matrix as a result of combining graphene oxide and reduced graphene. *Int J Polym Sci* 2013:493147. <https://doi.org/10.1155/2013/493147>
- Serodre T, Oliveira N, Miquita D et al (2019) Surface silanization of graphene oxide under mild reaction conditions. *J Braz Chem Soc* 30. <https://doi.org/10.21577/0103-5053.20190167>
- Gu Y, Guo Y, Wang C et al (2017) A polyamidoamine dendrimer functionalized graphene oxide for DOX and MMP-9 shRNA plasmid co-delivery. *Mater Sci Eng C* 70:572–585. <https://doi.org/10.1016/j.msec.2016.09.035>
- Ferrari AC, Basko DM (2013) Raman spectroscopy as a versatile tool for studying the properties of graphene. *Nat Nanotechnol* 8:235–246. <https://doi.org/10.1038/nnano.2013.46>
- Cançado LG, Takai K, Enoki T et al (2006) General equation for the determination of the crystallite size  $L_a$  of nanographite by



- Raman spectroscopy. *Appl Phys Lett* 88:1–4. <https://doi.org/10.1063/1.2196057>
27. Stefan-van Staden RI, Gheorghe DC, Ilie-Mihai RM et al (2021) Stochastic biosensors based on N- and S-doped graphene for the enantioanalysis of aspartic acid in biological samples. *RSC Adv* 11:23301–23309. <https://doi.org/10.1039/D1RA02066H>
  28. Ngo HT, Nguyen MTT, Do DP et al (2020) Low operating voltage resistive random access memory based on graphene oxide–polyvinyl alcohol nanocomposite thin films. *J Sci: Adv Mater Devices* 5:199–206. <https://doi.org/10.1016/j.jsamd.2020.04.008>
  29. Pokhrel J, Bhorla N, Anastasiou S et al (2018) CO<sub>2</sub> adsorption behavior of amine-functionalized ZIF-8, graphene oxide, and ZIF-8/graphene oxide composites under dry and wet conditions. *Microporous Mesoporous Mater* 267:53–67. <https://doi.org/10.1016/j.micromeso.2018.03.012>
  30. Balzar D (1993) X-ray diffraction line broadening: modeling and applications to high-T<sub>c</sub> superconductors. *J Res Natl Inst Stand Technol* 98:321. <https://doi.org/10.6028/jres.098.026>
  31. Jun SC (2015) Fundamental of Graphene. In: Rashid bin Mohd Yusoff, A. (ed) *Graphene-based energy devices*, pp. 1–48. Hoboken, NJ, John Wiley & Sons. <https://doi.org/10.1002/9783527690312.ch1>
  32. Li J, Cui J, Yang J et al (2016) Silanized graphene oxide reinforced organofunctional silane composite coatings for corrosion protection. *Prog Org Coat* 99:443–451. <https://doi.org/10.1016/j.porgcoat.2016.07.008>
  33. Khaled KF, Atta AA, Abdel-Shafi NS (2014) A structure/function study of polyamidoamine dendrimer as a steel corrosion inhibitor. *J Mater Environ Sci* 5:831–840
  34. Shuanger S, Zhiming Z, Liangmin Y (2017) Hydrophobic poly-aniline/modified SiO<sub>2</sub> coatings for anticorrosion protection. *Synth Met* 233:94–100. <https://doi.org/10.1016/j.synthmet.2017.10.002>
  35. McDonagh C, Sheridan F, Butler T, MacCraith BD (1996) Characterisation of sol-gel-derived silica films. *J Non-Cryst Solids* 194:72–77. [https://doi.org/10.1016/0022-3093\(95\)00488-2](https://doi.org/10.1016/0022-3093(95)00488-2)
  36. Jiang Z, Jiang Z, Tian X et al (2014) Amine-functionalized holey graphene as a highly active metal-free catalyst for the oxygen reduction reaction. *J Mater Chem A* 2:441–450. <https://doi.org/10.1039/C3TA13832A>
  37. Ramezanzadeh M, Ramezanzadeh B, Sari MG et al (2020) Corrosion resistance of epoxy coating on mild steel through poly-amidoamine dendrimer-covalently functionalized graphene oxide nanosheets. *J Ind Eng Chem* 82:290–302. <https://doi.org/10.1016/j.jiec.2019.10.025>
  38. Both J, Szabó G, Katona G et al (2022) Tannic acid reinforced sol-gel silica coatings for protection of zinc substrates. *Mat Chem Phys* 282:1–11. <https://doi.org/10.1016/j.matchemphys.2022.125912>

**Publisher's Note** Springer Nature remains neutral with regard to jurisdictional claims in published maps and institutional affiliations.

Springer Nature or its licensor (e.g. a society or other partner) holds exclusive rights to this article under a publishing agreement with the author(s) or other rightsholder(s); author self-archiving of the accepted manuscript version of this article is solely governed by the terms of such publishing agreement and applicable law.